ISSN 1995-0780, Nanotechnologies in Russia, 2015, Vol. 10, Nos. 1–2, pp. 25–33. © Pleiades Publishing, Ltd., 2015.
Original Russian Text © B.I. Shapiro, A.S. Mikhailov, M.I. Morgan, A.E. Baranchikov, V.K. Ivanov, 2015, published in Rossiiskie Nanotekhnologii, 2015, Vol. 10, Nos. 1–2.

Synthesis of Inorganic Dyes Based on Plasmonic Silver Nanoparticles for the Visible and Infrared Regions of the Spectrum

B. I. Shapiro[a], A. S. Mikhailov[a], M. I. Morgan[a], A. E. Baranchikov[b], and V. K. Ivanov[b,c]

[a] *Lomonosov State University of Fine Chemical Technology, pr. Vernadskogo 86, Moscow, 119571 Russia*
[b] *Kurnakov Institute of General and Inorganic Chemistry, Russian Academy of Sciences, Leninskii pr. 31, Moscow, 119991 Russia*
[c] *National Research Tomsk State University, pr. Lenina 36, Tomsk, 634050 Russia*
e-mail: bishapiro@mail.ru

Received April 14, 2014; in final form, October 23, 2014

Abstract—The effect of various technological factors during the multistage synthesis of plasmonic silver particles in aqueous solutions on nanoparticle size, morphology, and color is studied. The synthesized suspensions are found to contain tabular silver nanoparticles of hexagonal and triangular shape. The foundations of the technology for synthesizing stable silver colloids with a high silver concentration for the visible and near-infrared regions of the spectrum are developed.

DOI: 10.1134/S1995078015010176

INTRODUCTION

Metallic nanoparticles are characterized by a strong and specific interaction with electromagnetic radiation. The absorption spectra of small metallic particles contain an intense band that is absent in the spectra of large samples. This band is caused by the collective excitation of conduction-band electrons (surface plasmon polaritons) and its presence in the visible portion of the spectrum is responsible for the unique color of diluted colloidal dispersions of particles of a number of metals [1].

Plasmonics is a new physical technology that may replace the conventional technologies used in modern computers. The plasmonic-based logic devices will operate much faster and have a much greater information capacity than conventional electronic circuits. Furthermore, they will be much smaller than the existing optical systems [1–5]. The use of metallic nanoparticles makes it possible to tune the frequency of surface plasmon resonance by varying their size and shape. Low energy loss during the excitation of surface plasmon allows one to design miniature waveguides based on nanorods, nanowires, and ordered nanoparticles systems to transmit optical vibrations in nanodevices. Furthermore, compositions based on silver and gold nanoparticles can be used as plasmonic ink in electronic engineering and optoelectronic applications of printed electronics.

The use of plasmonic silver nanoparticles to kill cancer tumors is of significant interest. Nanoparticles injected into the blood flow are concentrated in a fast growing tumor [6]. Laser light heats nanoparticles by exciting resonance electron vibrations in them. High temperature kills tumor cells, while the adjacent healthy tissues remain intact [6].

Colored sols of silver and gold nanoparticles can be regarded as promising inorganic dyes for the visible and near-infrared region of the spectrum, since their molar extinction coefficient is rather high due to plasmon resonance. The estimated molar extinction coefficient of gold particles 40 nm in diameter is significantly higher than that for organic dyes in the same spectrum region [7]. Higher stability compared to that of organic dyes is an important advantage of plasmonic dyes based on noble metals. It is a known fact that silver-based photographs can be stored for over a century.

There are chemical and physical methods for producing silver and gold nanoparticles [1–5, 8–18]. The chemical methods for synthesizing silver and gold nanoparticles in a solution are the best-developed ones. They are based on the reduction of Ag^{+} and Au^{+3} ions by various reducing agents. A lot of studies have been devoted to chemical methods for synthesizing silver nanoparticles and their plasmonic properties [8–18]. They typically deal with the microanalytical synthesis of small amounts of silver. The aim of this study was to elaborate a method for the massive crystallization of silver nanoparticles of different sizes, morphologies, and colors.

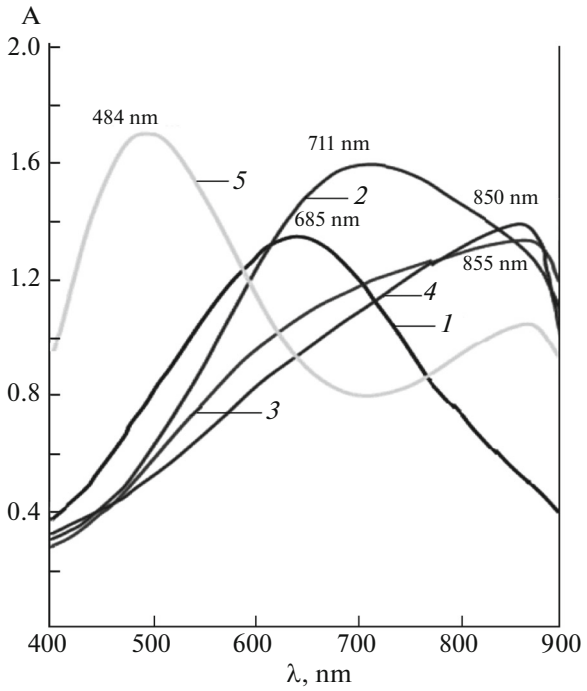

Fig. 1. Absorption spectra of gelatin layers of silver nanoparticles for different starting $AgNO_3$ concentrations: (*1*) 1.5×10^{-1} M, (*2*) 0.75×10^{-1} M, (*3*) 0.37×10^{-1} M, (*4*) 0.18×10^{-1} M, and (*5*) 0.09×10^{-1} M. The initial sol (*1*) was diluted 70-fold with a water–gelatin solution; the remaining sols (*2*)–(*5*) were diluted in accordance with $AgNO_3$ content during synthesis.

OBJECTS OF STUDY AND EXPERIMENTAL TECHNIQUES

Back in the 1930s, colored silver nanoparticles were used in the technology of photographic materials as filter dyes [19] (i.e., long before the concepts "nanotechnology" and "plasmonic metallic particles" appeared). The chemical synthesis of silver nanoparticles used in photography was employed in this study. This method included several stages and consisted in the sequential addition of silver nitrate and reducing agents, hydroquinone and Na_2SO_3, to alkaline gelatin solution at an elevated temperature [20].

$AgNO_3$ of reagent grade and an alkaline solution of inert gelatin of photography grade (Kazan Photogelatin Plant, Russia), batch no. 25866, were used. Bidistilled water was used to prepare aqueous solutions of silver sols. The suspension was synthesized in a 500 mL thermostated stainless steel reactor. The reaction mixture was stirred on a mechanically controlled stirrer. The total synthesis procedure lasted 26 min.

After synthesis, the suspension was cooled in a refrigerator, grounded, and sequentially washed with cold distilled water. After washing, the cooled suspension was melted at 43–45°C, supplemented with a 50% phenol solution, and stored in a refrigerator. To prepare colored gelatin layers, the nanoparticle suspension was diluted with an aqueous gelatin solution and poured onto glass (5 mL of suspension per 100 cm^2).

The absorption spectra of silver nanoparticle suspensions poured onto glass were recorded on a Beckman DU-8B spectrophotometer (United States). The nanoparticle size and shape were determined on a Carl Zeiss NVision 40-38-50 scanning electron microscope (Germany).

RESULTS AND DISCUSSION

The first experimental run of synthesis of silver nanoparticles (7.8 wt % gelatin, 1.5×10^{-1} M silver nitrate, 7×10^{-3} M hydroquinone and 4×10^{-2} M sodium sulfite) at 45°C and stirring rate of 400 rpm

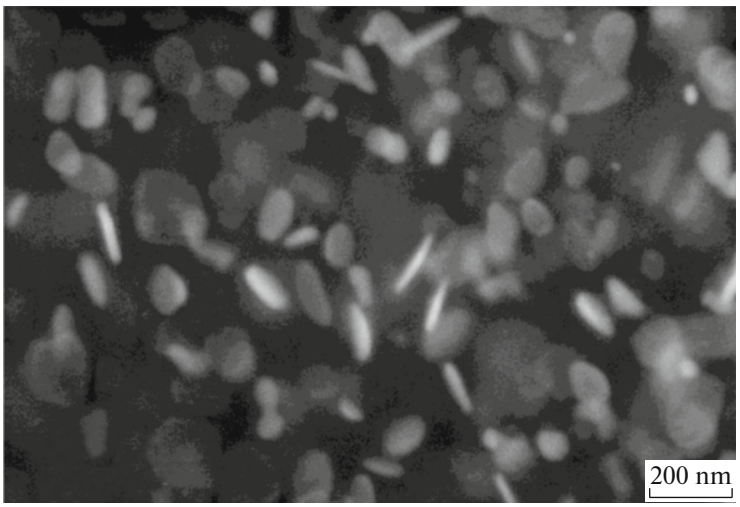

Fig. 2. SEM image of silver nanoparticles synthesized at 1.5×10^{-1} M $AgNO_3$ concentration in the reaction mixture.

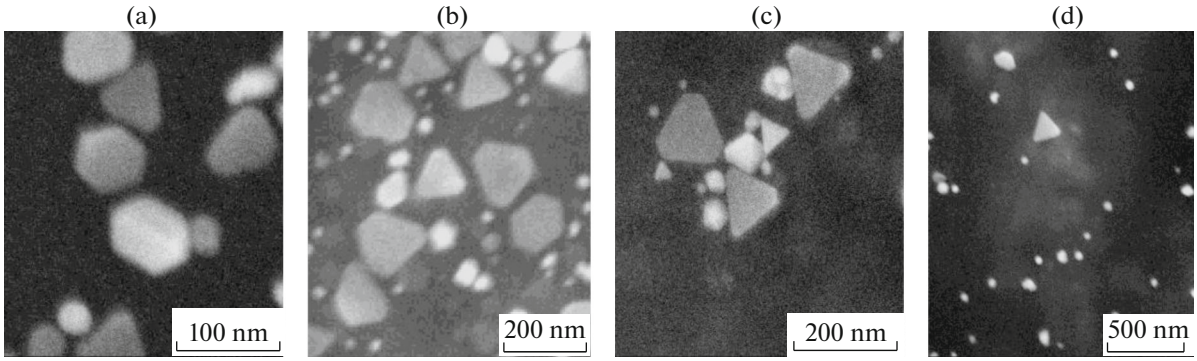

Fig. 3. SEM image of silver nanoparticles synthesized at $AgNO_3$ concentrations in the reaction volume: (a) 1.5×10^{-1} M, (b) 0.75×10^{-1} M, (c) 0.18×10^{-1} M, and (d) 0.09×10^{-1} M.

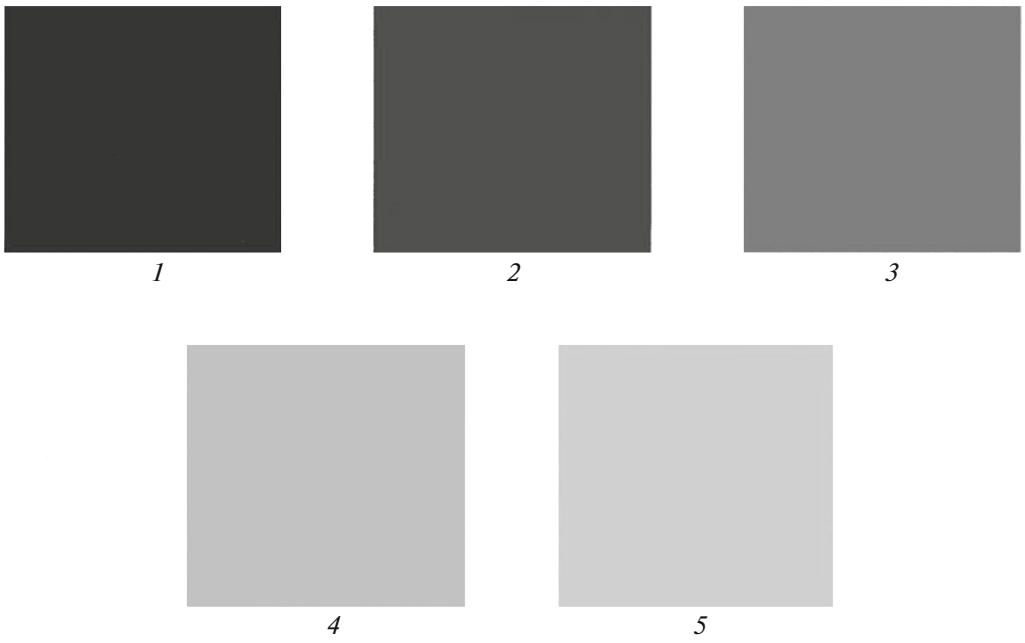

Fig. 4. Color of the samples of gelatin layers containing silver nanoparticles synthesized at different $AgNO_3$ concentrations in the reaction volume: (*1*) 1.5×10^{-1} M, (*2*) 0.75×10^{-1} M, (*3*) 0.37×10^{-1} M, (*4*) 0.18×10^{-1} M, and (*5*) 0.09×10^{-1} M.

showed that suspension samples with silver concentration of 16 g/L were of a deep blue color. Figure 1 (curve *1*) shows the absorption spectrum of the gelatin layer of nanoparticles (the initial sol was diluted 70-fold) with λ_{max} = 685 nm. This experimental run will subsequently be used as the control. According to the SEM data shown in Fig. 2, Ag nanoparticles were of a tabular shape (T-crystals) with a broad size distribution of particles.

It should be mentioned that the tabular anisotropic shape of silver nanocrystals is untypical in terms of crystallography, since the crystal lattice of silver is a high-symmetry fcc lattice. Hence, one would expect that isotropic nanoparticles rather than anisotropic are formed. These anisotropic shapes for silver nanoparticles have been described in literature in detail (e.g., review [18]). However, chemical synthesis most frequently gives rise to isometric ball-shaped silver nanoparticles with their plasmon absorption bands lying in the shorter wave region of the spectrum, ~400–500 nm. The variety of shapes of silver nanoparticles seems to be related to the large number of stages of the crystallization process and to the effect of synthesis conditions at the nucleation and particle-growth stages. Hence, the effects of certain synthesis parameters (namely, concentrations of silver nitrate and gelatin, type of reducing agent, stirring rate, and

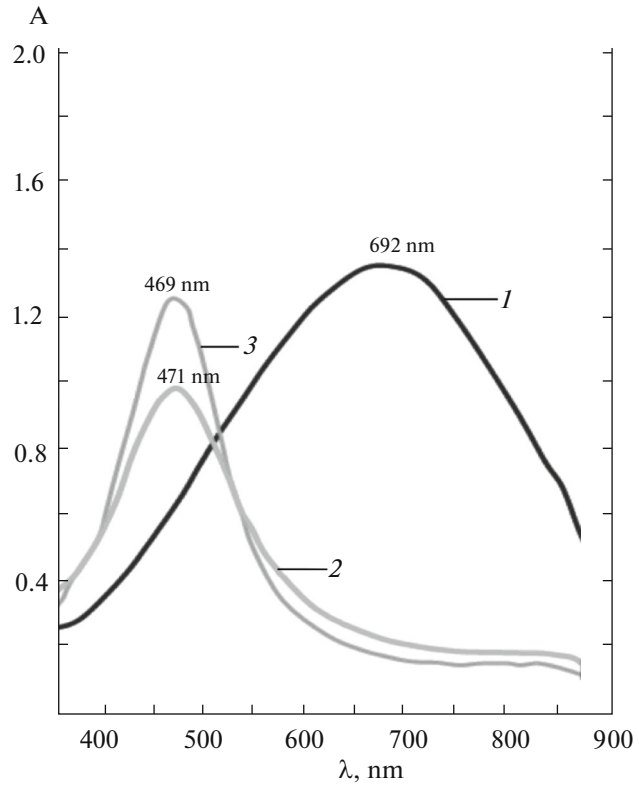

Fig. 5. Absorption spectra of silver nanoparticle layers at different gelatin concentrations during the synthesis (wt %): (*1*) 7.8, (*2*) 3.9, and (*3*) 1.9.

temperature) on nanoparticle morphology and color were studied more thoroughly.

Figure 1 shows the absorption spectra of silver nanoparticles sols for different $AgNO_3$ starting concentrations in the range from 1.5×10^{-1} M to 0.09×10^{-1} M. All other synthesis parameters were identical to those in the control experimental run. When $AgNO_3$ concentration was reduced from 1.5×10^{-1} M to 0.18×10^{-1} M, the absorption maximum shifted from the visible region of the spectrum toward the near-infrared region, from 685 nm to 850 nm (Fig. 1, curves *1*–*4*).

According to Fig. 3a, most silver nanoparticles synthesized at a $AgNO_3$ concentration of 1.5×10^{-1} M are tabular hexagons and triangles with the average size of ~100–110 nm (with hexagons predominating). The polydispersity and multiformity of particles give rise to a broad absorption band at $\lambda_{max} = 685$ nm, while the significant content of hexagonal particles is responsible for the blue color of suspension and gelatin layers.

The color of suspension samples poured as several layers onto the glass is shown in Fig. 4. A hypsochromic shift in the main absorption band (Fig. 1, curve *5*; $\lambda_{max} = 484$ nm) and the emergence of a second band with lower intensity at $\lambda_{max} = 853$ nm are observed at the minimal $AgNO_3$ concentration (0.09×10^{-1} M). The sample abruptly becomes yellow (Fig. 4, sample 5).

According to the SEM data, the change in spectral parameters of layers in the concentration range from 1.5×10^{-1} M to 0.18×10^{-1} M (Figs. 3a–3c) is associated with the increase in content of triangular particles and increase in particle size. This fact agrees with the bathochromic shift in plasmon bands as the nanoparticle shape is changed from hexagonal to triangular [1, 18]. The absorption spectrum containing two bands and the yellow color of the sample with the minimal $AgNO_3$ concentration (0.09×10^{-1} M) are caused by a significant content of small nanoparticles 30–40 nm in size (Fig. 3d). The long-wavelength band at $\lambda_{max} = 853$ nm is attributed to triangular particles ~200 nm in size.

The effect of the gelatin concentration on nanoparticle morphology and color was studied next. Figure 5 shows the absorption spectra of silver layers at three gelatin concentrations in the reaction mixtures (7.8, 3.9, and 1.9 wt %). All other synthesis parameters were identical to those in the control experimental run. Curve *1* describes the control run with gelatin concentration in the reaction volume of 7.8 wt % ($\lambda_1 = 692$ nm). A two- and fourfold reduction of gelatin concentration (Fig. 5, curves *2* and *3*) caused an abrupt hypsochromic shift in plasmon bands ($\lambda_2 = 471$ nm, $\lambda_3 = 469$ nm). The color of the layers changed from blue to purple and brownish (Fig. 6). According to SEM data, the reduction of gelatin concentration during synthesis gives rise

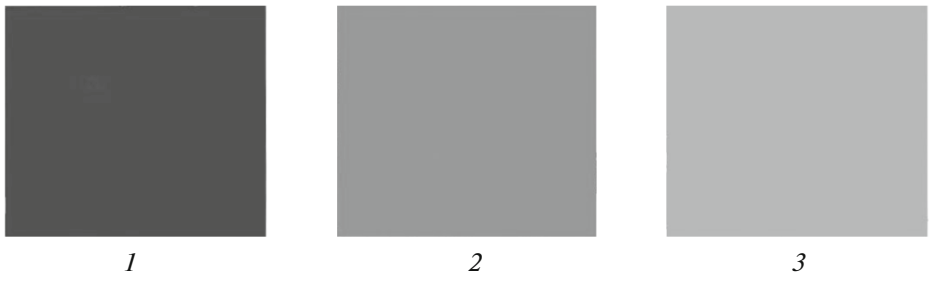

Fig. 6. Color of the layers containing silver nanoparticles synthesized at different gelatin concentrations in the reaction volume (wt %): (*1*) 7.8, (*2*) 3.9, and (*3*) 1.9.

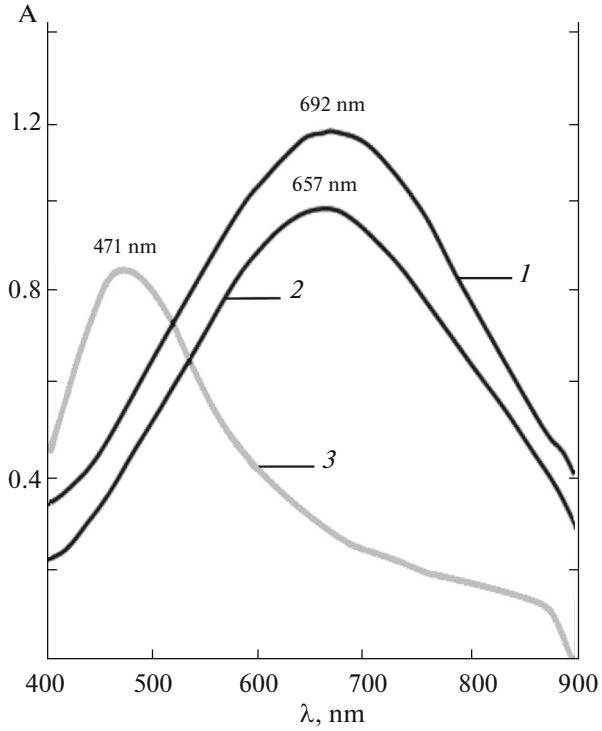

Fig. 7. Absorption spectra of silver nanoparticles for different reducing agents: (*1*) hydroquinone, (*2*) pyrocatechol, and (*3*) methol.

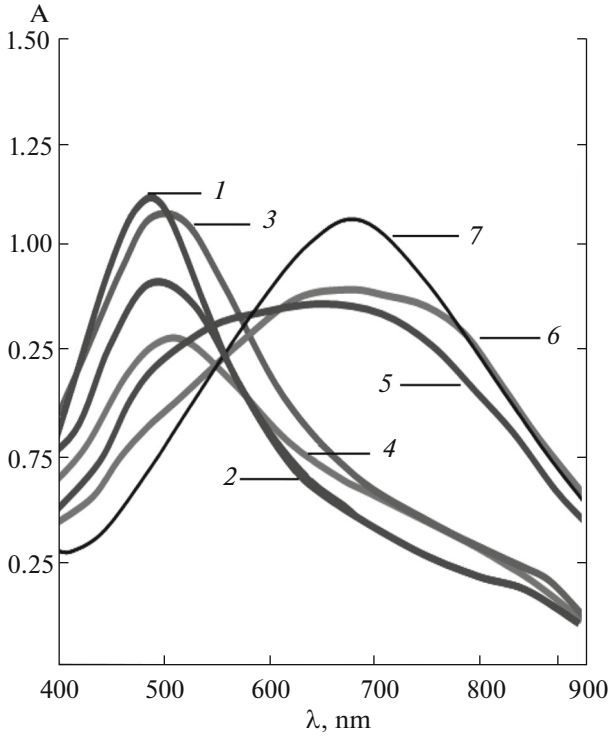

Fig. 8. Absorption spectra of silver nanoparticles at different stirring rates *n* (rpm) during synthesis: (*1*) 0, (*2*) 50, (*3*) 100, (*4*) 200, (*5*) 300, (*6*) 400, and (*7*) 600.

to smaller silver nanoparticles (~50–70 nm), mostly of a hexagonal shape.

Figure 7 shows the electronic absorption spectra of the layers of suspensions of nanoparticles synthesized using three different reducing agents; two of those are hydroxyl derivatives of benzene (hydroquinone and pyrocatechol) and the third reducing agent is a para-aminohydroxyl derivative of benzene (methol). The reducing agents were used at concentrations of 7×10^{-3} M. All other synthesis parameters were identical to those in the control experiment. Absorption spectra evidently show that the replacement of hydroquinone with pyrocatechol causes a certain hypsochromic shift in the absorption maximum of the layer, while the use of methol results in a significant hypsochromic shift in the absorption maximum. Hence, blue layers (samples 1 and 2) become yellow (sample 3). The reducing potential decreases in the series of the compounds

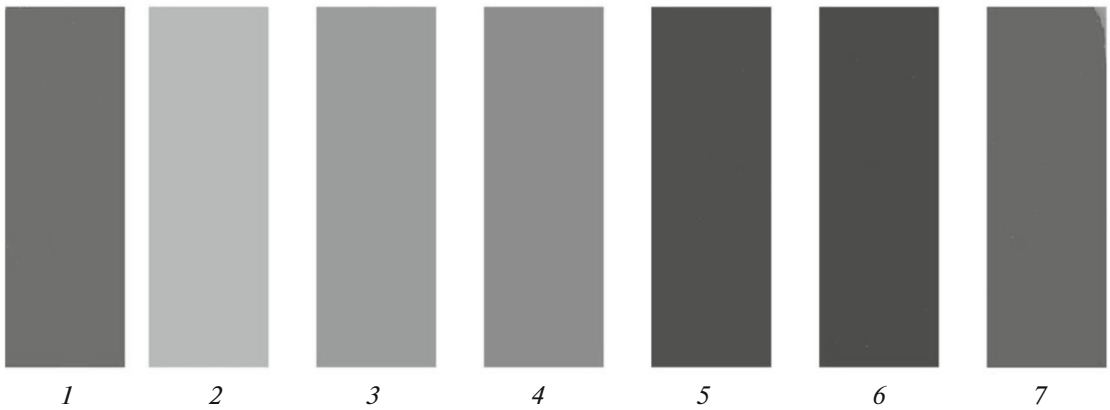

Fig. 9. Color of the layers containing silver nanoparticles synthesized at different stirring rates (rpm) during synthesis: (*1*) 0, (*2*) 50, (*3*) 100, (*4*) 200, (*5*) 300, (*6*) 400, and (*7*) 600.

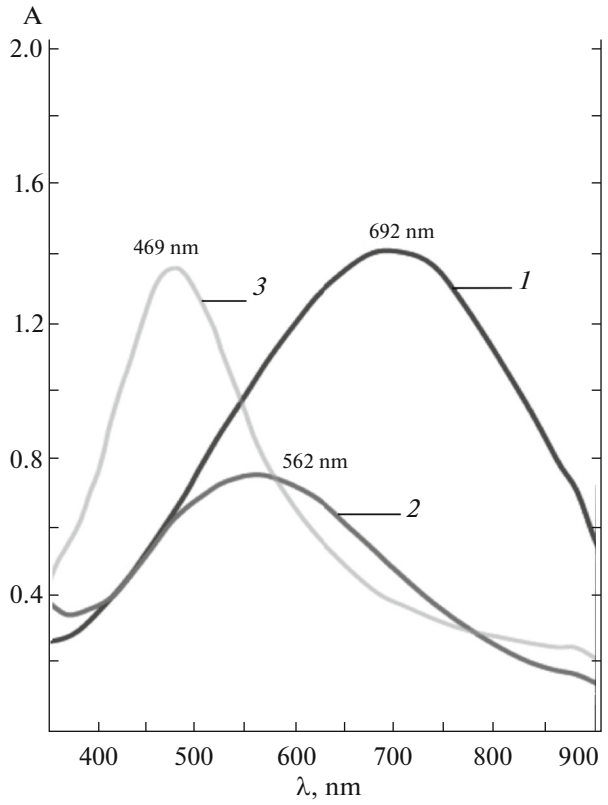

Fig. 10. Absorption spectra of silver nanoparticles at different synthesis temperatures (°C): (*1*) 45, (*2*) 60, and (*3*) 80.

under study [21], which may affect the rate of silver formation in the solution and, therefore, the morphology and color of silver nanoparticles.

The effect of the stirring rate on color of silver nanoparticles is of special interest. The stirring rate in the reactor (*n*) was measured from 0 (no stirring) to 600 rpm. All other synthesis parameters were identical to those in the control experiment. Figure 8 shows that an increase in the stirring rate causes a bathochromic shift in the absorption curves of silver layers and changes the width of the absorption bands. The broad color range of the resulting inorganic dyes based on silver nanoparticles is shown in Fig. 9.

Finally, Fig. 10 shows data on the effect of synthesis temperature on the formation of silver nanoparticles. Synthesis temperature was varied within the range of 45–80°C. All other synthesis parameters were identical to those in the control experiment. As follows from the data in Fig. 10, an increase in the temperature of synthesis causes a hypsochromic shift in the absorption band of plasmonic silver particles, which is particularly significant at 80°C. The colors of the corresponding layers are shown in Fig. 11.

Thus, it has been demonstrated that anisotropic tabular silver nanoparticles are formed in most experiments; particle morphology is to a great extent determined by synthesis parameters.

The formation of anisotropic tabular microcrystals was previously observed for silver halides, which also have a high-symmetry fcc crystal lattice [22]. Tabular AgHal microcrystals are 0.01–0.03 μm thick, while the ratio between the diameter and thickness of a microcrystal can be as high as 500: 1. They are usually synthesized at a large excess of KBr (pBr = 0.9–1.3) during AgBr synthesis. The interest in these crystals has abruptly increased after the Kodak company launched new, improved, color and black-and-white photo materials containing ultrathin AgHal microcrystals to the market in the early 1980s. Methods for synthesizing tabular AgCl, AgBr and AgBr(I) crystals [22] have been developed. The growth of tabular crystals is attributed to the formation of twinned crystals and increased growth rate along the twinning planes. The growth of twinned crystals and emergence of different forms of tabular crystals (triangles, hexagons, and truncated triangles) was first explained in [23]. The crystals preferentially grow along the twinning planes, because the latter form a re-entrant corner at the microcrystal surface, and the inclusion of ions into a re-entrant dihedral corner is preferable than inclusion into a facet (Fig. 12). Several twinning planes are typically formed and the lateral facets of the growing crystals turn out to be jagged. So-called polysynthetic

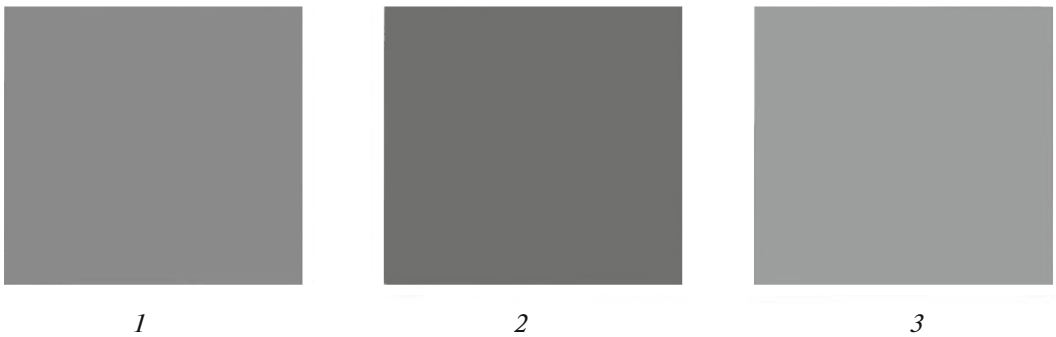

Fig. 11. Color of the layers containing silver nanoparticles synthesized at different synthesis temperatures (°C): (*1*) 45, (*2*) 60, and (*3*) 80.

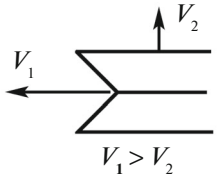

Fig. 12. Scheme of tabular crystal growth along the twinning plane.

twins with jagged defects are formed. The growth rate of lateral facets is considered to depend on the number of reentrant corners **n** and to be equal to $V = \mathbf{n} \cdot V_o$, where V_o is the growth rate of a lateral facet with a single re-entrant corner [23].

According to the modern conceptions, the growth of tabular silver halide crystals includes two sequential stages: (1) the formation of twinned crystals during the coalescence of nucleating microcrystals, usually with (111) faceting, and (2) the growth of twinned nuclei along the twinning planes [24]. The second stage is the key one; it depends on gelatin content, reagent feeding rate, stirring rate, and pAg. The coulomb attraction of oppositely charged nucleating microcrystals is the main reason for twinning.

Maskasky [25] used luminescent labeling to thoroughly trace grain evolution during its growth. These data were combined with the data on the number of twinning planes in tabular microcrystals of different shapes and the following scheme of microcrystal growth has been proposed.

A growing crystal with two twinning planes needs to contain wedge/groove re-entrant structures with A and B structures alternating along the perimeter (Fig. 13a). It is clear that the symmetries of A and B structures and the number of re-entrant corners are identical; hence, the rates of their lateral growth will be identical as well (i.e., this microcrystal will be of hexagonal shape) (Fig. 13a). If another twinning plane is added to this "even" tabular crystal, two types of lateral facet structures are possible: twinning planes are added below (Fig. 13b) and above (Fig. 13c). The crystal eventually acquires a triangular shape in both cases, since the facets with a large number of re-entrant corners (two corners on facets B (Fig. 13b) and A (Fig. 13c)) grow faster than the corresponding facets with the smaller number of re-entrant corners (one corner on facets A (Fig. 13b) and B (Fig. 13c)). It is evident that the addition of extra twinning plane to any of microcrystal varieties having odd number of planes gives rise to lateral facets with identical symmetry and number of re-entrant corners and equal growth rates, which again causes the formation of hexagonal microcrystals (Fig. 13d).

Thus, a conclusion can be drawn that hexagonal microcrystals grow for the even number of twinning planes (Figs. 13a, 13d), while an odd number of twinning planes gives rise to triangular microcrystals

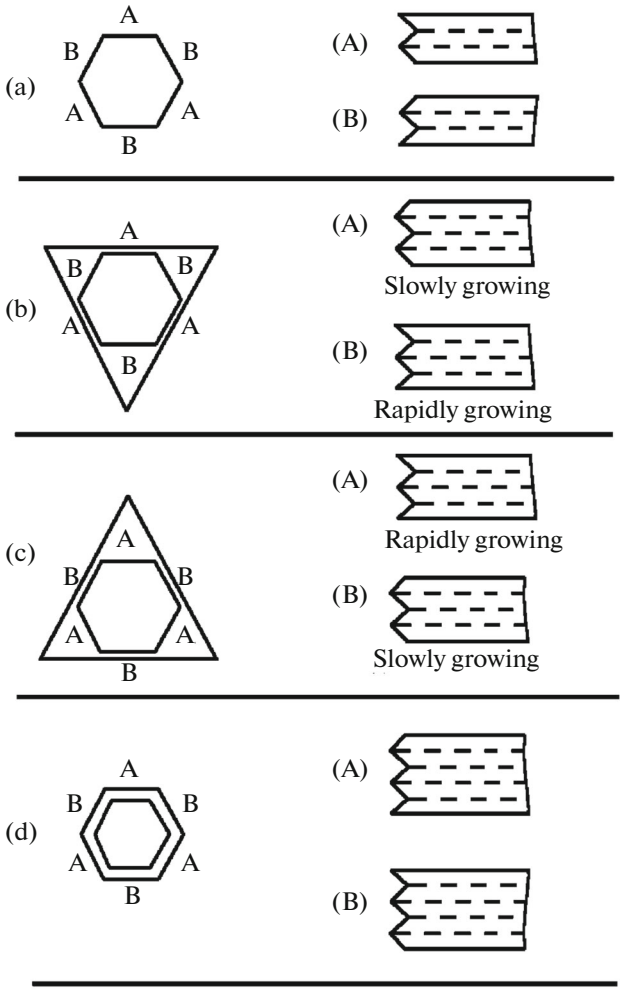

Fig. 13. Stable shapes of tabular AgHal microcrystals and structures of re-entrant corners (wedge/groove) A and B on lateral facets of growing microcrystals: (a) with two twinning planes, (b) with the third twinning plane located above, (c) with the third twinning plane located "below," and (d) with four twinning planes.

(Figs. 13b, 13c). It is also clear that intermediate forms—triangles truncated to various degrees—can be either "undergrown" triangles or "uncompleted" hexagons and thus may contain both even and odd numbers of twinning planes. These simple speculations lead to understanding why hexagonal crystals (probably with two twinning planes) prevail in the conventional photographic emulsions with tabular microcrystals. It is the smallest number among the possible numbers of twinning planes resulting in the formation of a re-entrant corner; thus, it is the most probable one. The chances that a third plane with a finite triangular grain shape is formed are much lower. One can assume that the twinning of nuclei plays a crucial role in growth of tabular hexagonal and triangular silver nanoparticles as well. This approach was discussed in [18, 26].

The growth of silver particles in the synthesis method under consideration is a complex multistage process that includes several sequential stages. The primary stage of the process seems to include Ag_2O nucleation in the alkaline $AgNO_3$ solution. Ag_2O was shown to play a special role in the formation of tabular silver nanoparticles [27–29]; it has been clearly demonstrated that the interaction of Ag_2O and hydrogen in an aqueous suspension gives rise to tabular hexagonal and triangular silver nanoparticles. The bathochromic shift in the plasmon absorption band of silver nanoparticles is usually caused by transition from spheroidal particles 30–50 nm in diameter to tabular faceted nanocrystals 80–150 nm in size. It was found in [30] that spheroidal silver nanoparticles have plasmon absorption bands in the range of 400–500 nm, pentagonal ones at 500–570 nm, and triangular particles in the range of 530–710 nm. Evanoff et al. [27–29] suggested that the low water solubility of Ag_2O (0.053 g/L at 80°C) and, hence, low concentration of silver ions in the solution are the main reason for formation of tabular crystals. As a result, silver particles grow very slowly.

The mechanism under consideration suggests that the initial process, twinning of nucleating $(Ag_2O)_n$ nanoparticles, is followed by the reduction of twinned $(Ag_2O)_n$ to silver yielding twinning planes of silver nanoparticles and by the subsequent growth of tabular silver particles along the twinning surfaces as silver ions in the solution are reduced. This mechanism is illustrated by the following scheme:

$$AgNO_3 + NaOH = AgOH + NaNO_3, \quad (1)$$

$$2\,AgOH = Ag_2O + H_2O, \quad (2)$$

$$nAg_2O = (Ag_2O)_n, \quad (3)$$

$$(Ag_2O)_n + mRed + xAg^+ = (Ag^0)_{2n+x} + mOx. \quad (4)$$

The effect of stirring rate on the morphology of silver nanoparticles may be associated with the twinning of nuclei in $(Ag_2O)_n$. Meanwhile, decrease in $AgNO_3$ concentration may affect both the number of twinning planes and the crystal growth rate along the twinning planes.

If hydroquione was used as a reducing agent, the order of the reactions of reduction of silver ions in the solution in the presence of Na_2SO_3 can be as follows [22]:

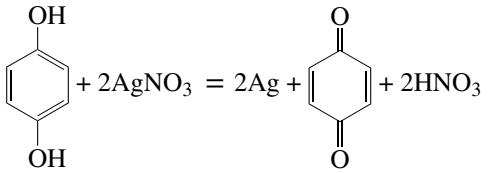

(5)

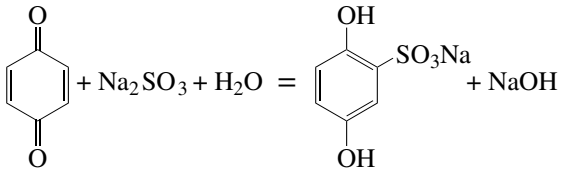

(6)

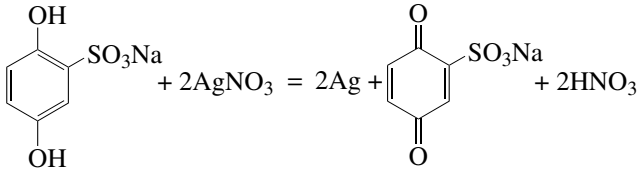

(7)

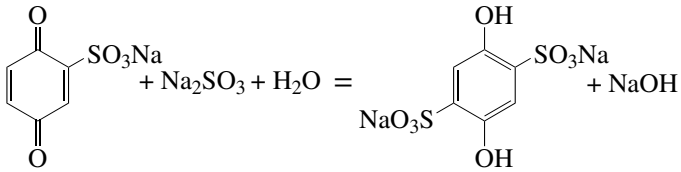

(8)

Thus, an initial hydroquione molecule can repeatedly reduce silver ions due to the sulfation of the resulting quinones. This fact explains why hydroquinone is used at a much lower concentration than $AgNO_3$. The tentative role of adsorption of negatively charged organic compounds onto certain facets of

nucleating silver nanoparticles, resulting in the inhibition of growth of these facets and anisotropic crystal growth in a direction parallel to these facets, has been discussed in literature (see review [18]). Thus, gelatin molecules are expected to play a special role in Ag crystal growth as they become negatively charged due to their carboxylic groups in the alkaline environment. Indeed, our experiments have proved that gelatin plays the key role in growth of tabular Ag nanocrystals. Sulfoderivatives of quinones that are formed from a reducing media comprising hydroquinone and sodium sulfite may also significantly contribute to the modification of the surface of growing Ag crystals (see the scheme of the process).

CONCLUSIONS

The effect of various technological factors during the multistage synthesis of silver nanoparticles on size, morphology, and color of nanoparticles has been studied. The resulting suspensions contain tabular silver nanoparticles of hexagonal and triangular shapes. The morphology of silver nanoparticles and color of plasmonic particles can be changed within a broad range by varying synthesis conditions. The foundations of the method for synthesizing stable water–gelatin sols of silver nanoparticles with high silver concentrations (up to 16 g/L) have been elaborated for the entire visible and near-infrared regions of the spectrum.

ACKNOWLEDGMENTS

The authors are grateful to E.Yu. Bulychev for his assistance in conducting the experiment and discussing results.

REFERENCES

1. V. V. Klimov, *Nanoplasmonics* (Fizmatlit, Moscow, 2009) [in Russian].
2. V. I. Roldugin, Usp. Khim. **69**, 899 (2000).
3. B. G. Ershov, Ros. Khim. Zhurn. (Zn. Ros. Khim. Obshch. im. D. I. Mendeleeva) **45**, 20 (2001).
4. Yu. A. Krutyakov, A. A. Kudrinskii, A. Yu. Olenin, and G. V. Lisichkin, Usp. Khim. **77**, 242 (2008).
5. B. N. Khlebtsov, V. A. Khanadeev, V. A. Bogatyrev, L. A. Dykman, and N. G. Khlebtsov, Nanotech. Russ. **4** (7–8), 453 (2009).
6. R. K. Jain and T. Stylianopoulos, Nat. Rev. Clin. Oncol. **7**, 653 (2010).
7. R. K. Jain, K. S. Lee, and I. H. El-Sayed, J. Phys. Chem. B **110**, 7238 (2006).
8. M. A. Noginov, G. Zhu, A. M. Belgrave, R. Bakker, V. M. Shalaev, E. E. Narimanov, S. Stout, E. Herz, T. Suteewong, and U. Wiesner, Nature **460**, 1110 (2009).
9. P. K. Jain and M. A. El-Sayed, Chem. Phys. Lett. **487**, 153 (2010).
10. N. Kometani, M. Tsubonishi, T. Fujita, K. Asami, and Y. Yonezawa, Langmuir **17**, 578 (2001).
11. I. S. Lim, F. Goroleski, D. Mott, N. Kariuki, W. Ip, J. Luo, and Ch.-J. Zhong, J. Phys. Chem. B **110**, 6673 (2006).
12. V. S. Lebedev, A. G. Vitukhnovsky, A. Yoshida, N. Kometani, and Y. Yonezawa, Colloids. Surf. A **326**, 204 (2008).
13. A. Yoshida, Y. Yonezawa, and N. J. Kometani, Langmuir **25**, 6683 (2009).
14. A. Yoshida and N. Kometani, J. Phys. Chem. C **114**, 2867 (2010).
15. W. Ni, H. Chen, J. Su, Zh. Sun, J. Wang, and H. Wu, JACS Commun. **132**, 4806 (2010).
16. J. Hranisavljevic, N. M. Dimitrijevic, G. A. Wurtz, and G. P. Wiederrecht, JACS Commun. **124**, 4536 (2002).
17. A. Yoshida, N. Uchida, and N. Kometani, Langmuir **25**, 11802 (2009).
18. J. E. Millstone, S. J. Hurst, G. S. Métraux, J. Cutler, and C. A. Mirkin, Small **5**, 646 (2009).
19. *Color Cinematography,* Ed. by E. M. Goldovskii (Iskusstvo, Moscow, 1955) [in Russian].
20. *Process Regulations no. 6-17-276 for Synthesizing Photographic Emulsion for Color Negative and Positive Films* (Industrial Group Tasma Named after V. V. Kuibyshev, 1986).
21. *The Theory of the Photographic Process,* Ed. by T. James (Macmillan, 1977).
22. B. I. Shapiro, *Theoretical Foundations of Photographic Process* (Editorial URSS, Moscow, 2000) [in Russian].
23. R. W. Berriman and R. H. Herz, Nature **180**, 293 (1957).
24. M. G. Antoniades, J. S. Wey, J. Imag. Sci. Technol. **39**, 323 (1995).
25. J. E. Maskasky, J. Imag. Sci. **31**, 15 (1987).
26. C. Lofton and W. Sigmund, Adv. Funct. Mater. **15**, 1197 (2005).
27. D. D. Evanoff and G. Chumanov, J. Phys. Chem. B **108**, 13948 (2004).
28. D. D. Evanoff and G. Chumanov, J. Phys. Chem. B **108**, 13957 (2004).
29. D. D. Evanoff and G. Chumanov, Chem. Phys. Chem. **6**, 1221 (2005).
30. J. J. Mock, M. Barbic, D. R. Smith, D. A. Schultz, and S. Schultz, J. Chem. Phys. **116**, 6755 (2002).

Translated by D. Terpilovskaya